


Retention Model and Express Retention Test of Ferroelectric HfO₂-Based Memory

Vitalii Mikheev, Ekaterina Kondratyuk[✉], and Anastasia Chouprik^{✉*}

Moscow Institute of Physics and Technology, 9 Institutskiy Lane, Dolgoprudny, Moscow Region 141700, Russia

 (Received 13 July 2022; revised 20 October 2022; accepted 2 December 2022; published 27 December 2022)

Ferroelectric hafnium oxide films are one of the most promising functional materials for a new generation of nonvolatile memory for data storage because of a number of excellent performance features, including nanosecond speed, high endurance, low power consumption, full scalability, and perfect compatibility with Si technology. However, the commercialization of this memory is hindered by its limited retention time, which still does not meet the 10-year electronics-industry standard. To date, much effort has been focused on the improvement of retention via material and interface engineering. Meanwhile, the evaluation and comparison of engineering results have been hampered, since there is still no unified retention test. Indeed, a specific feature of the retention performance is that it cannot be measured directly, because 10 years is required to measure the actual polarization loss. In this paper, we present a physical model that predicts the retention loss in HfO₂-based memory during long-term information storage. The time-dependent polarization loss originates from the phenomenon of polarization imprint, which consists in the temporal development of a preferential polarization state in a poled ferroelectric. For high reliability of the retention calculation, the model takes into account the specific features of imprint evolution in the ferroelectric material HfO₂. Among these is the origin of the imprint in this material, which consists in the interplay of two physical mechanisms, specifically, charge injection into interface traps and migration of mobile charged defects across the functional layer. The second property of HfO₂ taken into account is the different rates of imprint evolution in two types of HfO₂ film that exist within each memory cell. These two types of film originate from two populations of domains that appear during crystallization of the HfO₂ and persist during the whole lifetime of the memory cell. The high accuracy of the retention model makes it possible to implement an express retention test, i.e., to predict the retention time in record short time (1 h) for any particular sample, whereas usually a retention test takes at least several days. For Hf_{0.5}Zr_{0.5}O₂-based capacitors, the retention model shows excellent agreement with experimental results. The proposed model can serve not only for the implementation of this express retention test, but also as a tool for intelligent material engineering in the field of nonvolatile ferroelectric memory.

DOI: [10.1103/PhysRevApplied.18.064084](https://doi.org/10.1103/PhysRevApplied.18.064084)

I. INTRODUCTION

The discovery of ferroelectric properties in HfO₂ thin films [1] has opened up an opportunity to implement complementary-metal-oxide-semiconductor-compatible ferroelectric random access memory (FRAM) that offers attractive performance features such as excellent scalability, nanosecond speed, low power consumption, and record endurance. However, the commercialization of this type of memory has been hampered, mainly due to limited retention time. A developed memory can be implemented by the electronics industry only if it exhibits a standard retention time of 10 years at temperatures in the industrial range from -40 to 85 °C.

The retention time is determined by the phenomenon of ferroelectric aging [2], which manifests itself in hafnium oxide in a change of the coercive voltage with time due to a gradual increase in the internal bias field across the ferroelectric layer. The accompanying effect of a gradual shift of the P - V hysteresis along the V axis is called the imprint. Because of an increase in the imprint over time, the amplitude of a predefined readout voltage pulse may turn out to be close to the mean coercive voltage. This causes a decrease in the fraction of switched ferroelectric domains and thus a possible readout failure.

The retention issues are the most challenging and most urgent tasks from the point of view of microelectronic applications of ferroelectric hafnium oxide. Specifically, two main challenges need to be addressed for the successful implementation and commercialization of HfO₂-based FRAM. First, a material stack that meets all

*chouprik.aa@mipt.ru

industry requirements (including good retention time) must be designed by means of material and interface engineering. Second, a reliable method of long-term prediction of the polarization readout over the storage time needs to be developed. Until then, it will be difficult to evaluate the results of the design of the materials. A specific feature of the retention performance is that it cannot be measured directly, because it would take 10 years to measure the actual retention loss. The usual way to predict polarization loss in HfO₂-based memory devices consists in linear interpolation of the experimental dependence of the read polarization on the logarithm of the storage time to a time of 10 years [3–6]. However, this approach has no physical basis.

A prediction method can be reliable only when it is physically grounded, i.e., the method must take into account the physical mechanisms of ferroelectric aging. Several physical mechanisms have been proposed for perovskite ferroelectrics: (i) alignment of dipolar defects in the bulk of the ferroelectric [7,8], (ii) thickening of an interface nonferroelectric dead layer due to oxidation of the electrodes and a local phase transformation to a nonferroelectric phase [9], (iii) migration of charged defects due to drift or diffusion [10,11], and (iv) charge injection and subsequent charge trapping by interface traps [12–14]. The mechanism associated with the injection of charge into the ferroelectric layer underlies a retention model that shows good agreement with experiment for Pb(Zr, Ti)O₃ (PZT) ferroelectric capacitors [13]. Hafnium oxide has a number of specific properties, which must be taken into account for accurate calculation of the retention loss. For example, due to the relatively high mobility of oxygen vacancies in hafnium oxide [15], the ferroelectric aging of this material is associated with the interplay of two phenomena—charge injection into defect traps (followed by charge trapping) and spatial redistribution of mobile charged defects inside the ferroelectric layer [16]. Another important feature is the existence of two types of HfO₂ film within a memory device structure, which originate from two populations of domains that appear during crystallization of the HfO₂ and persist in the memory cell during its lifetime [8]. The rate of ferroelectric aging differs for these two types of film, which needs to be taken into account for accurate prediction of the retention loss.

In this paper, we present a retention model that predicts the loss of polarization readout during long-term information storage. Because it takes into account the specific properties of the material, this prediction method is highly accurate and thus allows one to implement a fast retention test. Specifically, the method allows one to obtain information about the retention time for any particular sample in approximately 1 h, whereas usually a retention test takes several days. For Hf_{0.5}Zr_{0.5}O₂-based capacitors with small leakage, the retention model shows excellent agreement with experimental results.

II. RETENTION MODEL

The proposed method is developed and tested using Si/W/TiN/Hf_{0.5}Zr_{0.5}O₂(10 nm)/TiN/Al capacitors. W(40 nm)/TiN(10 nm) bottom and TiN(20 nm)/Al(150 nm) top electrode films are grown by magnetron sputtering and electron-beam evaporation. A Hf_{0.5}Zr_{0.5}O₂ (HZO) film is grown via thermal atomic layer deposition at a 280 °C substrate temperature, using Hf[N(CH₃)(C₂H₅)₄], Zr[N(CH₃)(C₂H₅)₄], and H₂O as precursors and N₂ as a carrier and purging gas. Crystallization of the HZO film into the ferroelectric structural phase occurs during post-metallization rapid thermal annealing for 30 s at 600 °C in Ar. To wake up the as-prepared Hf_{0.5}Zr_{0.5}O₂ film, the ferroelectric capacitors are cycled 10⁶ times by applying trapezoidal pulses with an amplitude of 3.5 V and a duration of 30 μs.

Since ferroelectric aging is a thermally induced effect, and thus the retention state deteriorates with an increase in temperature, the verification of the retention test is done at the upper limit of the industrial range (85 °C). In this way, we obtain information about the worst retention time under the worst conditions among those of practical interest.

A. Components of the polarization loss

Generally, the polarization loss during readout after some time of storage may originate from either thermal depolarization or the imprint effect, or both. Thermal depolarization is a reverse polarization switching driven by the depolarization field occurring in a poled ferroelectric film capacitor. This contribution may be significant or even dominant in PZT [17]. An effect of thermal depolarization was reported for Al-doped HfO₂ as well [18]. In contrast, in a HZO film, thermal depolarization is minuscule, and the polarization loss is determined only by the imprint effect [16].

The imprint effect produces several components of polarization loss. Precisely, during aging, four charge components modify the initial switchable polarization P_0 acquired during readout before the beginning of aging. Specifically, the minimum readout polarization P_{read} is equal to $P_0 - Q_1 - Q_2 + Q_3 - Q_4$. In this expression, the charge components are taken with their absolute values, and thus a minus sign before a charge component means that it decreases the switchable polarization during readout, while the plus sign before the component Q_3 indicates that it increases the readout polarization. Let us consider the origin of the charge components.

Thermal conditioning of the HZO capacitor in the downward polarization state causes a shift of the switching I - V curve towards positive voltages [Fig. 1(a)]. As a result, the polarization current peak may occur partially beyond the amplitude of the readout voltage pulse [e.g., 3 V in Fig. 1(a)]. This means that the coercive voltage of some part of the domains exceeds the readout voltage, and these

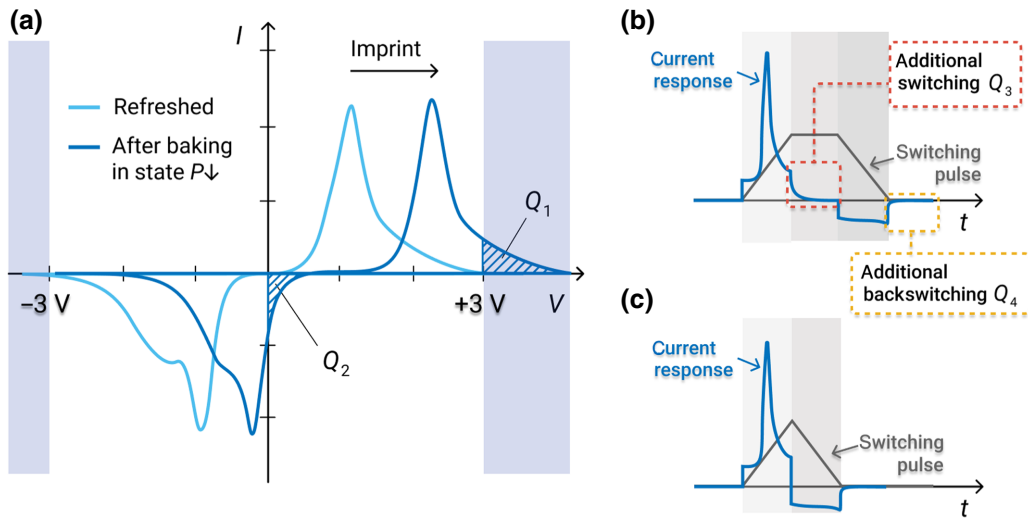


FIG. 1. (a) Switching I - V curves of a capacitor in downward polarization state before and after conditioning the sample at elevated temperature. Transient currents during application of either (b) trapezoidal or (c) triangular switching pulses to the aged capacitor.

domains will not switch during readout. The area under the I - V curve denoted by Q_1 corresponds to the polarization reversal charge of these domains. This component decreases the switchable polarization and, therefore, is taken with a minus sign in the expression for P_{read} . Obviously, the charge loss Q_1 strongly depends on the amplitude of the readout pulse and decreases with an increase in the pulse amplitude. However, a small read voltage amplitude is preferable, to minimize power consumption and maximize endurance.

The second component of the polarization loss (Q_2) is associated with the backswitching of a part of the polarization. During the readout pulse, in some part of the domains the polarization switches twice. In these domains, during the front tail of the pulse, the polarization switches to a direction determined by the polarity of the readout voltage and then, during the back tail, it switches to the initial direction. The charge Q_2 flowing during backswitching has the opposite sign to P_0 and thus is subtracted from P_0 and suppresses the switchable polarization. For this reason, the absolute value of Q_2 is taken with a minus sign in the expression for P_{read} .

In the case of triangular read pulses, the retention loss is determined mainly by the contributions Q_1 and Q_2 . However, the retention of FRAM has historically been tested with trapezoidal pulses. It is worth noting that the pulses used in memory chips are neither triangular nor trapezoidal, but have an irregular shape [6]. However, during the design of functional stacks with the required retention performance, any pulse shape will do. In order to be able to compare the results with those of other groups, we follow the generally accepted approach and use trapezoidal pulses.

Trapezoidal readout pulses induce an additional contribution (Q_3) to the polarization readout. In transient

currents corresponding to a trapezoidal pulse, one can observe a nonzero current flowing during the flat part of the voltage pulse [Fig. 1(c)], although the displacement current due to the linear capacitance is zero here. The charge Q_3 corresponds to an additional switching of polarization compared with a triangular pulse. This additional switching originates from the limited speed of polarization reversal at low field in the ferroelectric layer. A decrease in the switching speed with a decrease in the amplitude of the switching pulse and/or its duration is a fundamental property of the polarization-switching kinetics of polycrystalline ferroelectric films [19]. Meanwhile, the internal built-in field across the ferroelectric film, \mathbf{E}_{bi} , which develops with aging, is aligned opposite to the applied switching field, \mathbf{E}_{appl} . Thus, the total electric field in the ferroelectric layer, \mathbf{E}_{tot} , is smaller than the applied switching field ($\mathbf{E}_{\text{tot}} = \mathbf{E}_{\text{appl}} + \mathbf{E}_{\text{bi}}$) and decreases with time. As a result, for a predefined readout pulse, the switching speed decreases with time [20], and the contribution of the additional “kinetics” switching, Q_3 , becomes larger and larger. Since this component is an additional switching of polarization during the readout procedure, it increases the readout polarization and, therefore, is taken with a plus sign in the expression for P_{read} .

The fourth component of the polarization loss (Q_4) is also associated with the internal built-in field and the limited switching speed at small voltages. After the passage of the switching voltage pulse, the internal built-in field \mathbf{E}_{bi} persists in the ferroelectric, and $\mathbf{E}_{\text{tot}} = \mathbf{E}_{\text{bi}}$. The built-in field causes further backswitching of the polarization, which, with a zero applied field, lasts for some time. The reason for including this component (Q_4) with a minus sign in the expression for P_{read} is explained in Sec. II D. It is noteworthy that due to the relatively small magnitude of \mathbf{E}_{bi} and the polarization-switching-kinetics law,

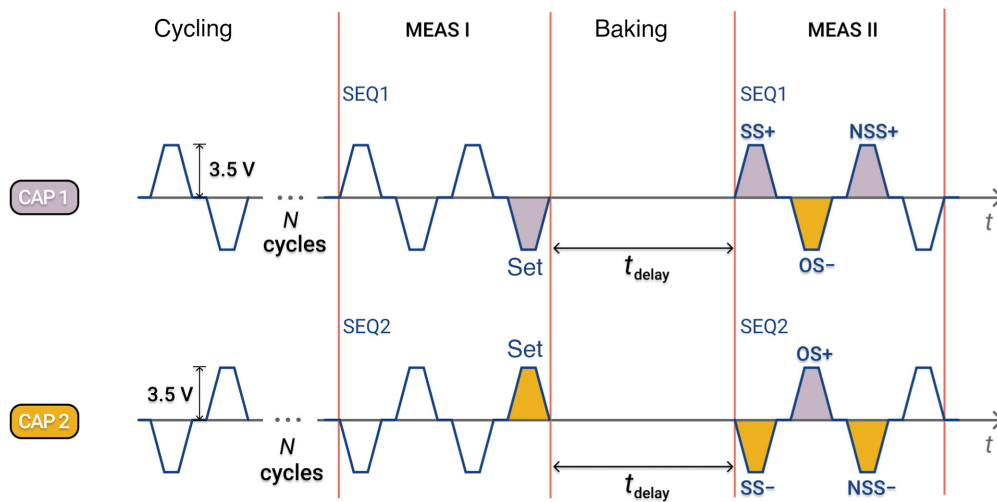


FIG. 2. Voltage pulse sequences used for same-state (SS), new-same-state (NSS), and opposite-state (OS) retention tests. The read polarization corresponds to integrated current responses, as notated. Integration of the current response is done during the complete transient range of the trapezoidal pulse.

this process could take quite a long time (approximately $10 \mu\text{s}$) compared with the time delays in real memory chips.

Obviously, the components Q_3 and Q_4 do not manifest themselves in the I - V curves, and can be detected only in transient currents.

B. Experimental dataset for the retention test

In 2010, voltage pulse sequences for characterization of the retention time of PZT-based FRAM were developed [21]. These sequences were later utilized for retention tests of Si-doped HfO_2 [22]. The sequences are universal, i.e., they were designed to measure retention loss due to both thermal depolarization and the imprint effect. Since the retention loss in HZO is caused solely by the imprint effect, we simplify the voltage pulse sequence.

We use two sequences with opposite polarity to get retention data for readout pulses of different polarity (Fig. 2). For each experimental point for the polarization readout after storage, we take a fresh structure. After the wake-up procedure, we apply the sequence SEQ1 or SEQ2 and simultaneously measure the current response (MEAS I). The last pulse of this sequence serves as a set pulse, i.e., it switches the capacitor to either an upward or a downward polarization state. After some delay t_{delay} corresponding to the storage time, we repeat the sequence and once again measure the current response (MEAS II). Since the history of the applied voltage and of the delays between pulses strongly modifies the rate of the aging process [16], we accurately maintain definite pulse durations and time delays. The delay between the cycling procedure and MEAS I is equal to the duration of the pulse tails, the flat part of the pulses, and the delay between pulses in the sequence ($10 \mu\text{s}$ in the work presented here).

Full information about the current responses MEAS I and MEAS II during the retention test allows one to control the reliability of the retention test, which, due to the impact of history, depends on the repeatability of particular measurements. I - V curves reconstructed from the current transients are used for calculation of the retention loss.

It should be noted that baking can be carried out under either closed- or open-circuit conditions, i.e., while keeping the capacitor electrodes either connected or disconnected from the power supply. Previously, we studied the impact of this issue in detail and found that it does not affect the rate of aging [16]. The experimental data in the present work are obtained after baking under closed-circuit if the delay time is 1 min or less. For longer delay times, we carry out baking under open-circuit conditions.

C. Dynamics of the imprint

Since ferroelectric aging causes temporal evolution of the imprint, the rate of change of the coercive voltage is the basis for calculation of the polarization loss. Typically, the position of the current peak in the I - V curve is taken as the coercive voltage [13,16]. However, the coercive voltage obtained in this way is too approximate for reliable prediction of the retention loss. We propose a more accurate approach to measuring the coercive voltage.

1. Dynamics of the imprint within two types of HZO film originating from two populations of domains in as-prepared film

Comparing the I - V curves before and after baking, one can notice that the I - V curve not only shifts along the V axis but also changes its shape [Figs. 1(a) and 3(a)]. The current peak seems to be composed of two smaller current peaks

that shift independently of each other. When the positions of the small peaks are close to each other, the total peak looks like a single one. When the positions of the peaks are farther apart from each other, splitting of the I - V curve is clearly observed. Splitting of the I - V curve is a specific feature of as-prepared HZO capacitors, and it apparently disappears during the wake-up procedure.

The shape of the I - V curves is associated with the statistical distribution of the coercive voltage, and the splitting of the I - V curves is usually attributed to the existence of two opposite internal built-in fields. Each of these fields is specific to one of two types of HZO film, which are associated with two populations of domains that appear during the crystallization of the HZO. Grains, formed during crystallization, span the whole thickness of the HZO film [23–25], and so the domain structure is single-layered [Fig. 3(c)]. It has been experimentally shown that in an as-prepared HZO film, half of the film area has an upward polarization across the whole film thickness, while the other half has a negative downward polarization [23]. Immediately after preparation of the film, it begins to undergo unintentional ferroelectric aging, with the aging aggravating over time. Technological routines performed at elevated temperatures (e.g., lithographic patterning of the top electrodes) additionally accelerate the aging. As a result, internal bias fields build up in the HZO, and the direction of the local field is defined by the orientation of the polarization vector in that particular place in the film. Therefore, two populations of domains, with upward and downward polarizations, produce two opposite internal bias fields in the as-prepared film, which manifest themselves in splitting of the I - V curves.

During the first several thousand operating cycles of a HfO₂-based capacitor (the so-called wake-up process), the internal bias fields gradually reduce, possibly due to field-induced spatial redistribution of charged defects and/or release of injected charge by traps [10,14,23]. Note that this wake-up is the reverse effect to aging [26]. Although the initial internal fields disappear during wake-up, the two types of HZO film related to the initial domain structure persist [Fig. 3(c)]. In other words, the HZO film “remembers” its initial domain structure during the whole lifetime of the memory cell. One more indication of this “memory” phenomenon comes from the splitting of the I - V curve of cycled HZO that is observed during heating of the sample, as reported, e.g., in Ref. [27]. A number of hypotheses can explain the “memory” phenomenon; for example, the origin may be dead layers of slightly different thicknesses in the two types of domains formed in the as-prepared film. Meanwhile, one could imagine that after the formation of the initial domain structure during crystallization, different dead layers could be formed due to different rates of electrochemical redox reactions of the HZO with the electrode material in areas with a positive or negative interface polarization charge. In this case, the aging rates would differ

between these areas, as follows from the models described in this paper and in Refs. [12,13]. These models indicate that a thickness difference equal to or even less than one lattice constant is sufficient for significantly different aging rates [20]. Because of the different aging rates, the peaks shift along the V axis at different rates, and the total peak broadens and then splits. The effect of the deformation of the I - V curve needs to be taken into account in the prediction of the retention loss.

To reconstruct the I - V curve after the required storage time (e.g., 10 years), we determine the imprint rate for both types of HZO film. We acquire a series of I - V curves after different delays t_{delay} and fit separately their positive and negative branches by sums of two Gaussian distributions [Fig. 3(b)]. The positions of the Gaussian peaks, their amplitudes, and their widths are the arguments of the fit-discrepancy function. During the evolution of the imprint, the positions of the Gaussian current peaks change, while their amplitude and width should remain constant, because the proportion of each type of film is defined by the crystallization of the HZO and does not change over time. From the experimental points and their fitting in Fig. 3(b), it is evident that the imprint rate is indeed different for the two distributions of coercive voltage. Let us discuss the fitting function for the experimental coercive voltage.

2. Impact of both charge injection and migration of charged defects on the temporal evolution of the imprint

The time dependence of the voltage offset has been described theoretically by a nonlinear imprint model, which is based on charge injection through an interfacial layer [13]. The concept employed in this scenario suggests that in the ferroelectric film, the readout polarization gradually decreases due to the existence of an interfacial dielectric region located between the ferroelectric film and the metal electrode [Fig. 4(a)] [12,13]. In the poled state, this layer is exposed to a very high electric field that provokes charge injection into defect traps at the dielectric/ferroelectric interface [12,13], and this trapped charge causes the voltage offset observed during reversal of the polarization in the ferroelectric material. In the band diagram [Fig. 4(c)], it is evident how the polarization charge produces a potential well at the dielectric/ferroelectric interface. As mentioned above, the grains span the whole thickness of the film, and the domain structure is single-layered. Therefore, no additional factors affecting the potential energy profile in the HZO layer are expected. Figure 4(b) illustrates how the spatial distribution of the injected charge and the potential well evolve with time within the frame of the nonlinear imprint model. The effect of charge injection produces a logarithmic dependence of the voltage offset on time, $V_{c \text{ offset}} = V_0 \log(1 + t/t_0)$, where V_0 and t_0 are fitting parameters that characterize the rate and the moment that the voltage starts

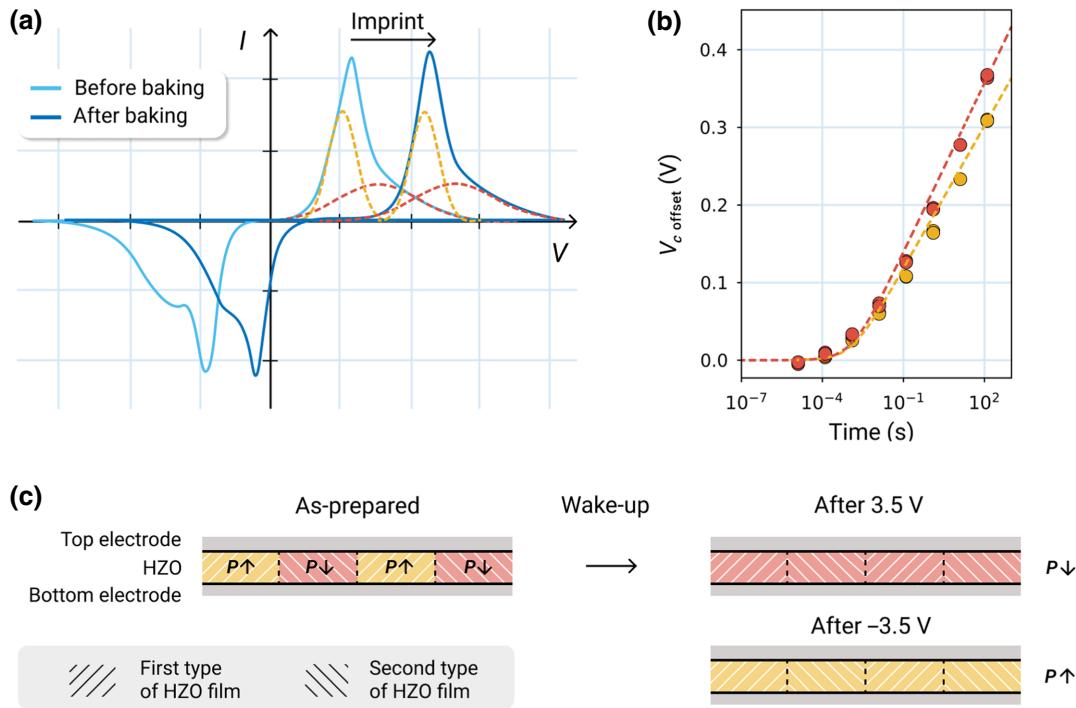


FIG. 3. Dynamics of the imprint in two types of HZO film. (a) Decomposition of the current response into two Gaussian functions. (b) Experimental points for the offset of the coercive voltage for the two types of HZO film, and fitting of the experimental dependence by the function $V_{c \text{ offset}} = V_0 \log^2(1 + t/t_0)$. On careful inspection, one can note that several (almost overlapping) experimental points are plotted for each storage time. In fact, the offset of the coercive voltage is acquired and plotted for four capacitors. (c) Cross section of ferroelectric HZO-based capacitor and the domain structure at different stages of capacitor operation.

to offset [13]. It is noteworthy that this formula works in the case of current transport described by an exponential dependence on voltage, e.g., thermionic emission with a Schottky contribution, the Poole-Frenkel mechanism, or cold field emission. However, the approximation of the experimental points in Fig. 3(b) by a simple logarithmic function $V_{c \text{ offset}} = V_0 \log(1 + t/t_0)$ does not give very good agreement (not shown in this paper). Specifically, the experimental voltage offset increases faster than what is given by a simple logarithmic function that is produced solely by the effect of charge injection. A much better fit is given by the steeper quadratic logarithmic function $V_{c \text{ offset}} = V_0 \log^2(1 + t/t_0)$ [Fig. 3(b)]. This indicates that on the time scale considered, some second physical mechanism [7,9–11,14] contributes additionally to the imprint effect and accelerates it.

Earlier, it was reported that the ferroelectric aging of HZO is caused by the interplay of two effects—trapping of injected charge by interface traps and migration of mobile charged defects towards the metal electrode [16]. The charged defects are usually attributed to positively charged oxygen vacancies V_O because they form at interfaces of HfO_2 -based devices with metals due to a redox reaction with the electrode material [15,23,26,28]. Oxygen vacancies in hafnium oxide have a relatively high mobility [15,29] and drift across the film following electric fields

[10,30], in particular, the electric field of the polarization charge that non-ideally screened by charges in electrodes. On the other hand, oxygen vacancies are charged traps that can trap the injected charge, becoming electrically neutral and thus stopping their movement. Therefore, the injected charge, which falls into the potential well formed by the polarization charge, is captured by charged oxygen vacancies that are mostly located near the interface and move slowly under the action of the electric field. Because of the smaller thickness and lower dielectric permittivity of the interfacial dielectric layer, the field across the dielectric is larger than the field in the ferroelectric [Fig. 4(c)]. Therefore, one should expect that oxygen vacancies move towards the metal electrode, and thus the effective thickness of the interfacial dielectric layer decreases. As a result, the injected charge could be localized not only strictly at the dielectric/ferroelectric interface but also nearby.

To simulate the evolution of the voltage offset caused by both injection of charge and migration of charged-defect traps, we numerically solve the following electrostatic and charge-transport equations for a ferroelectric capacitor with a thin passive dielectric layer located near the electrode [12,13]:

$$E_d d_d + E_f d_f = 0, \quad (1)$$

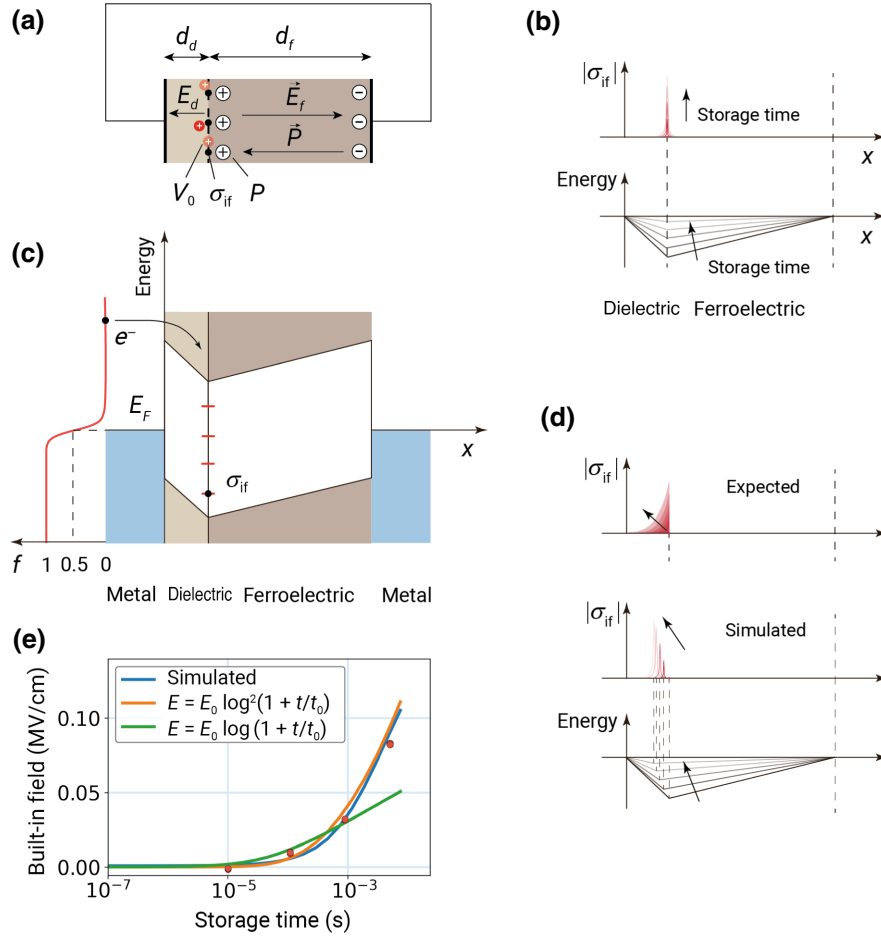


FIG. 4. (a) Sketch of structure consisting of interfacial dielectric and ferroelectric layers. (b) Spatial distribution of charge and corresponding profile of energy (bottom of the conduction band and top of the valence band in the dielectric and ferroelectric layers) in the frame of the model of pure charge injection. (c) Band diagram of the structure under closed-circuit conditions, and Fermi function aligned with the band diagram; f is the average number of electrons in a single-particle state. (d) Expected and simulated spatial distributions of charge, and corresponding profile of the energy (bottom of the conduction band and top of the valence band in the dielectric and ferroelectric layers) in the frame of the model of charge injection and charged-trap migration. (e) Dependence of the built-in electric field $V_{c \text{ offset}}$ on time: simulated in the frame of the model of charge injection and charged-defect migration, fitting of the simulated dependence with the formulas $V_{c \text{ offset}} = V_0 \log(1 + t/t_0)$ and $V_{c \text{ offset}} = V_0 \log^2(1 + t/t_0)$, and experimental points for one type of HZO film. In (b),(d), the black arrows indicate the evolution of the charge and potential-energy well over the storage time.

$$E_d \varepsilon_d + E_f \varepsilon_f = \frac{P + \sigma_{\text{if}}}{\varepsilon_0}, \quad (2)$$

where E_d , E_f , d_d , d_f , ε_d , and ε_f are the electric fields across the dielectric and ferroelectric layers, the thicknesses of the dielectric and ferroelectric layers, and the dielectric permittivities of the dielectric and ferroelectric layers, respectively; ε_0 is the vacuum permittivity, P is the polarization charge, and σ_{if} is the charge density injected into the interface traps. The injected charge is defined as

$$\sigma_{\text{if}} = \int_0^t J(E_d) dt. \quad (3)$$

We consider the situation where the charge transport through the dielectric layer is described by the Richardson-Dushman equation with a Schottky contribution (though, due to physical reasons, the Poole-Frenkel formula gives a very similar result):

$$J(E_d) = A_0^* T^2 \exp\left(-\frac{e\varphi_B}{k_B T}\right), \quad (4)$$

$$\varphi_B = d_d \left(E_d - \sqrt{\frac{eE_d}{4\pi n}} \right), \quad (5)$$

where $A_0^* = (4\pi e k_B m_{\text{eff}})/h^3$ is the Richardson constant, k_B is the Boltzmann constant, h is the Planck constant, e is the elementary charge, m_{eff} is the effective mass, T is the

temperature, $e\varphi_B$ is the potential barrier, and n is the optical dielectric permittivity of the dielectric layer.

The model of nonlinear imprint implies that the spatial position of the injected charge is constant, i.e., the spatial distribution of charge is described by a delta function [Fig. 4(b)]. If charged-defect traps migrate following the electric field across the dielectric layer towards the metal electrode and stop their movement after capture of the injected charge, the instantaneous spatial distribution of the injected charge can be qualitatively described as shown in Fig. 4(d). To simplify this situation and introduce it into the model equations, we assume that the displacement of the center of mass of the charge distribution is described by a velocity v equal to μE_{de} , where μ is the mobility of positively charged oxygen vacancies. Thus, $d_d = d_d^{\text{init}} - vt$, where d_d^{init} is the initial thickness of the interfacial dielectric layer and d_d is its instantaneous effective thickness. We assume that $d_f = d - d_d$, where $d = 10$ nm is the total thickness of the HZO.

The instantaneous built-in field $E_{\text{bi}}(t)$ produced by the injected charge σ_{if} is equal to

$$E_{\text{bi}}(t) = E_f(t) - E_f(0). \quad (6)$$

where $E_f(t)$ is the instantaneous real field in the ferroelectric. It can be calculated by means of numerical solution of the system of Eqs. (1)–(4), and it can also be expressed using them:

$$E_f = -\frac{(P + \sigma_{\text{if}}) d_f}{\varepsilon_0 \varepsilon_d d_f - \varepsilon_0 \varepsilon_f d_d} \frac{d_d}{d_f}, \quad (7)$$

where σ_{if} , d_d , and d_f are time-dependent variables. At $t = 0$, $\sigma_{\text{if}} = 0$ and $d_d = d_d^{\text{init}}$. The injected charge σ_{if} is determined by Eq. (3), which includes the time-dependent field across the dielectric layer,

$$E_d = \frac{(P + \sigma_{\text{if}}) d_f}{\varepsilon_0 \varepsilon_d d_f - \varepsilon_0 \varepsilon_f d_d}. \quad (8)$$

From the model of the interplay of charge injection and migration of charged defects, we obtain the simulated numerical dependence of the internal built-in field [blue line in Fig. 4(e)] with the following fixed parameters: $T = 85^\circ\text{C}$, $\varepsilon_f = 30$ [23], $m_{\text{eff}} = 0.11m_e$ [31], and $\mu = 10^{-12} \text{ cm}^2 \text{ V}^{-1} \text{ s}^{-1}$ [29]. Some parameters are free and are found by searching for the best agreement between the simulated dependence and the experimental data for the coercive-voltage offset: $\varepsilon_d = 16$, $e\varphi_B = 1.1 \text{ eV}$, $n = 7.1$, and $d_d^{\text{init}} = 0.6 \text{ nm}$. The values obtained are physically feasible for HZO [20,24,32], although they do not help to clarify the origin of the dead layer. Indeed, the value of ε_d obtained is equal to the dielectric permittivity of one of the polymorphs of hafnium oxide, specifically, the paraelectric monoclinic structural phase, which varies in the range from

16 to 20 [24]. In addition, this value is lower than ε_f , which is in agreement with the model of charge injection [12,13]. Meanwhile, it was shown previously that a HfO_2 film could include an interlayer formed by the nonferroelectric tetragonal phase, which has a larger dielectric permittivity. One of the possible explanations is that our HZO film does not contain a tetragonal interlayer, but the dead layer is simply an oxidized electrode interlayer or even a screening layer inside the electrode. This is indicated by the very small thickness of the dead layer, which is given by the calculations (2 lattice constants). In Fig. 4(e), we also show an attempt to fit the simulated dependence by two functions, $V_{c \text{ offset}} = V_0 \log(1 + t/t_0)$ and $V_{c \text{ offset}} = V_0 \log^2(1 + t/t_0)$. It is evident that the simulated numerical dependence is poorly approximated by the simple logarithmic law, and it is well (though not ideally) approximated by the quadratic logarithmic law.

Returning to the full experimental dataset in Fig. 3(b), we can see that the experimental points are in very good agreement with the function $V_{c \text{ offset}} = V_0 \log^2(1 + t/t_0)$. This function is used for separate fitting of the coercive-voltage dynamics in the two types of film, which are defined by the two populations of domains in the as-prepared HZO. The parameters of both fittings are used further to predict future coercive voltages in the two types of film. Because of the good fitting, we assume that for HZO this semiempirical function is more accurate than a simple logarithm for the calculation of the retention loss. It should be noted that experimental data on coercive voltages are usually obtained after some hundreds or thousands of minutes of baking, if one counts from the starting point of the development of the imprint. Points measured after such long baking times can indeed be fitted by a simple logarithm (of course, with other V_0 and t_0 values), as proposed by Tagantsev *et al.* [13]. Indeed, far from zero time, a simple and a quadratic logarithmic function are similar, or, specifically, a quadratic logarithmic function looks like a straight line on V - $\log t$ axes, whereas a simple logarithmic function is just a straight line.

The high accuracy of fitting the experimental dependence of $V_{c \text{ offset}}(t_{\text{delay}})$ now available allows us to significantly shorten the baking times and propose a fast (“express”) retention test. Using I - V curves acquired by means of the voltage sequence MEAS II after very short delays, we can accurately predict the offset of the coercive voltage, $V_{c \text{ offset}}$.

D. Pulsed P - V curve for calculation of polarization switching

Let us consider two ways to calculate the retention loss on the basis of the dynamics of the imprint. The first way is based on the reconstruction of the future I - V curve that would actually occur after the required storage time. The reconstruction of the positive current peak is

done by summing Gaussian peaks for both types of film, with new positions $V_{c1} = V_{c1 \text{ init}} + V_{c1 \text{ offset}}$ and $V_{c2} = V_{c2 \text{ init}} + V_{c2 \text{ offset}}$, where $V_{c1 \text{ init}}$ and $V_{c2 \text{ init}}$ are the initial coercive voltages, while the offset voltages are predicted by the dependences $V_{c1 \text{ offset}} = V_{0(1)} \log^2(1 + t/t_{0(1)})$ and $V_{c2 \text{ offset}} = V_{0(2)} \log^2(1 + t/t_{0(2)})$. Here, $V_{0(1)}$, $V_{0(2)}$, $t_{0(1)}$, and $t_{0(2)}$ are the parameters of fitting functions. The voltage parameters $V_{0(1)}$ and $V_{0(2)}$ are associated with the slope of the fitting curve and thus characterize the rate of increase of the imprint, while the time parameters $t_{0(1)}$ and $t_{0(2)}$ are related to the starting moment of the development of the imprint.

The charge ($P_0 - Q_1$) is calculated by integration of the reconstructed positive current response in the voltage range from 0 to V_{readout} , while the charge Q_2 is calculated by integration of the negative current response in the voltage range from V_{readout} to 0 [Fig. 1(a)]. The total readout polarization is equal to $P_{\text{read}} = P_0 - Q_1 - Q_2$. Note that all charges are taken with absolute values.

For triangular pulses, the results of this calculation are in good agreement with the experimental points (as shown in Sec. III). However, for trapezoidal pulses it is necessary to additionally calculate the charge Q_3 using some polarization-switching-kinetics model, which is outside the scope of this paper.

The second method is designed to avoid a computation of the “kinetics” charge Q_3 . To calculate the polarization loss, we use the pulsed P - V curve measured at 85°C in the following way. We take a fresh structure and start with electrical cycling with 10^6 bipolar pulses. The last pulse in the cycling sequence serves as a preset of the capacitor [Fig. 5(a)]. Then we apply a pulse with an amplitude equal to V_{readout} (3.5 V in the present work) and integrate the current flowing during this pulse. The measured charge is the maximum charge that corresponds to a complete polarization reversal. The maximum charge is equated to 1 relative unit (r.u.). In Fig. 5(b), it is used for normalization of other points of the P - V curve. To measure the next point, we refresh the structure with 100 bipolar pulses, apply a pulse with an amplitude smaller than V_{readout} by some ΔV , and measure the switched polarization. This procedure is repeated for a number of amplitudes in the range from V_{readout} to 0. For better statistics, we repeat the measurement of the whole dataset on another fresh structure and average the two datasets. The other branch of the pulsed P - V curve [Fig. 5(b)] is acquired in a similar way from two other fresh structures.

In general, the shape of the pulses can be arbitrary; e.g., it may imitate the shape of the readout pulse in real memory chips [6]. In the present work, we use trapezoidal switching pulses with a duration of the flat part of $10 \mu\text{s}$, whereas the duration of the tails is varied to maintain a constant voltage rate $dV/dt = 3.5 \text{ V}/10 \mu\text{s}$. The pulse with an amplitude of 3.5 V is exactly the same as the pulses used in the retention test. The delay between the preset

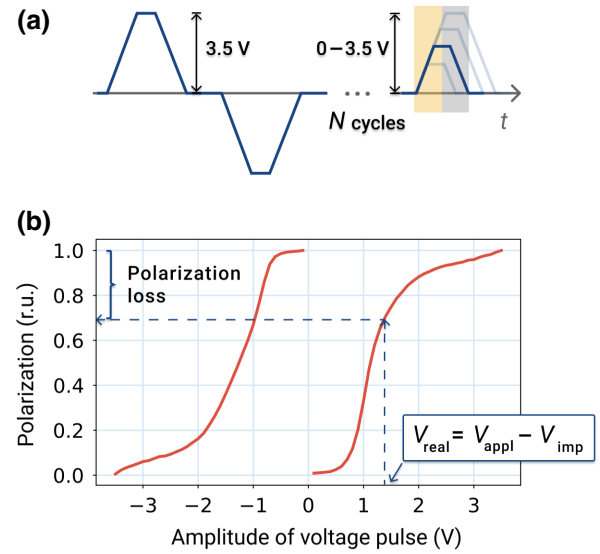


FIG. 5. (a) Voltage pulses used for pulsed- P - V -curve measurements. The two time intervals for current integration during the pulse shown by the bold line are highlighted in yellow and gray. (b) Pulsed P - V curve measured at 85°C with the pulse train shown in (a), representing the switching polarization as a function of the voltage amplitude of the switching pulse.

pulse and the switching pulse is chosen as $10 \mu\text{s}$ in order to avoid any contribution from the imprint. In fact, the imprint begins to develop 10^{-5} s after the preset [as is evident from Fig. 3(b)], and therefore this time value determines the maximum acceptable delay. In the absence of the imprint, the real field in the ferroelectric V_{real} is equal to the applied field V_{appl} , whereas after a delay of 10^{-5} s the imprint develops and thus an offset voltage appears. As a result, the real field in the ferroelectric decreases: $V_{\text{real}} = V_{\text{appl}} - V_{\text{offset}}$.

Since the two types of HZO film have different imprint rates, the effective offset of the coercive voltage is taken as

$$V_{c \text{ offset}} = V_{c1 \text{ offset}} \frac{A_1}{A_1 + A_2} + V_{c2 \text{ offset}} \frac{A_2}{A_1 + A_2}, \quad (9)$$

where $V_{c1 \text{ offset}}$ and $V_{c2 \text{ offset}}$ are the offsets of the coercive voltages of the two types of film, and A_1 and A_2 are the amplitudes of the Gaussian distributions of coercive voltages. Thus, we take into account the fact that a Gaussian distribution with a larger amplitude affects the effective coercive voltage more strongly. It should be noted that the effective offset of the measured coercive voltage is equal to the offset of any voltage applied to the ferroelectric capacitor, i.e., $V_{\text{offset}} = V_{c \text{ offset}}$.

The pulsed P - V curve is used to convert V_{real} into the readout polarization. In the first step, we find the charge loss ($Q_1 - Q_3$). For this purpose, we calculate the real voltage in the HZO during the passage of the readout voltage pulse, $V_{\text{real}} = V_{\text{appl}} - V_{\text{offset}} = V_{\text{readout}} - V_{\text{offset}}$.

Then, using the “conversion” P - V curve, we acquire the charge loss ($Q_1 - Q_3$), marked as the “polarization loss” in Fig. 5(b). In the second step, we find the component Q_4 in the same way. Let us refine the origin and role of this component. Polarization backswitching by the charge Q_4 takes place after the passage of the first (SS) pulse in the sequence MEAS II, i.e., at zero voltage (Fig. 2). That is, during the delay between the SS and OS pulses, the polarization switches slightly towards the state that would be induced by the OS pulse, and this decreases the readout of the polarization by the OS pulse. The component Q_4 is equal to the “polarization loss” of the conversion P - V curve at zero V_{appl} , i.e., at a real voltage equal to $V_{\text{real}} = -V_{\text{offset}}$.

It is noteworthy that the “polarization loss” found with the conversion P - V curve at V_{readout} does not include the backswitching component Q_2 , which is related to the polarization backswitching during the back tail of the readout pulse. Indeed, the curve is measured in such a way as to avoid any contribution of the imprint, i.e., with $V_{\text{real}} = V_{\text{appl}}$. For calculation of the latter component Q_2 , another method is employed. Specifically, it is calculated using the reconstructed future I - V curve in the way described above for the first method.

Let us summarize how to calculate the polarization readout for the same state and the opposite state using four polarization loss components. During the passage of the first (SS) pulse in the sequence MEAS II (Fig. 2), the polarization readout is equal to $P_{\text{SS}} = P_0 - Q_1 - Q_2 + Q_3$. After the passage of the SS pulse, additional backswitching by Q_4 takes place at zero voltage. That is, during the delay between the SS and OS pulses, the polarization switches slightly towards the state that would be induced by the OS pulse. Therefore, during the passage of the second (OS) pulse, the polarization readout is equal to $P_{\text{OS}} = P_0 - Q_1 - Q_2 + Q_3 - Q_4 = P_{\text{SS}} - Q_4$.

The general algorithms for the retention tests are summarized in Fig. 6. One can note that the second prediction method requires the use of the first method to obtain the component Q_2 , while the first method can be used alone. However, the first method does not allow one to obtain the Q_3 and Q_4 components. Therefore, the second method is more accurate but requires more effort. The second prediction method was proposed in outline by Tagantsev *et al.* [13], while we adapt it here for HZO-based FRAM taking into account the specific properties of this material, and develop an express retention test.

It should be noted that the pulsed P - V curve does not show ideal saturation at large voltage amplitudes [Fig. 5(b)], though good saturation is typical for stoichiometric HZO capacitors under standard ambient conditions. This effect is caused by the leakage current, which increases with temperature due to both thermionic emission and Poole-Frenkel mechanisms of current transport. Since the current is integrated during the full switching

pulse, the displacement current due to the linear capacitance is subtracted from itself, because it is positive in the rising pulse tail and negative in the falling tail. Meanwhile, the leakage current is the same in both tails and is nonzero in the flat part of the pulse. During integration, it is summed and contributes to the charge readout. We believe that the use of a P - V curve with a leakage contribution is the most feasible method if it is necessary to characterize the retention time under practical conditions of memory-chip applications, i.e., at the upper limit of the industrial temperature range. Indeed, at elevated operating temperatures, leakage contributes to the polarization charge readout in the way described above. However, if one needs to obtain the saturated P - V curve, one could remove the leakage-current contribution. For this purpose, one can divide the integration time interval into two intervals as shown in Fig. 5(a). The charge obtained in the first interval consists of three components—a switched polarization, a positive linear displacement charge, and a leakage charge—while the charge in the second interval consists of a negative linear displacement charge and a leakage charge. The difference of these charges is equal to the switched polarization with a constant linear displacement contribution, while the sum is the switched polarization with the leakage contribution. This method of measurement of the switching polarization using two time intervals can be useful for an advanced measurement of the polarization-switching kinetics that could be an alternative to the classical method [19,20].

III. VERIFICATION OF THE RETENTION MODEL

First, we examine the first retention test, which is based solely on the reconstruction of a future I - V curve, which would be expected after some storage time, and the subsequent calculation of the read polarization $P_{\text{read}} = P_0 - Q_1 - Q_2$. We obtain confirmation of the large impact of the “kinetics” charge Q_3 on the read polarization. Indeed, in the case of trapezoidal pulses, when the polarization switching continues by Q_3 during the flat part of the pulse, we have a large discrepancy between the experimental data and the calculated P_{read} [Fig. 7(a)]. In the case of triangular read pulses (when $Q_3 = 0$), the result of the calculation is in good agreement with the experiment. It is noteworthy that the experimental read polarization is smaller in the case of triangular pulses, which indicates that the effect of the limited speed of polarization switching plays an important role in the polarization readout, and that this effect manifests itself even more during long storage and thus for a large built-in field.

Further, we examine the second (main) retention test, which is based on both the conversion P - V curve and the reconstructed I - V curve. For this purpose, we examine which physical mechanism causes retention loss—charge

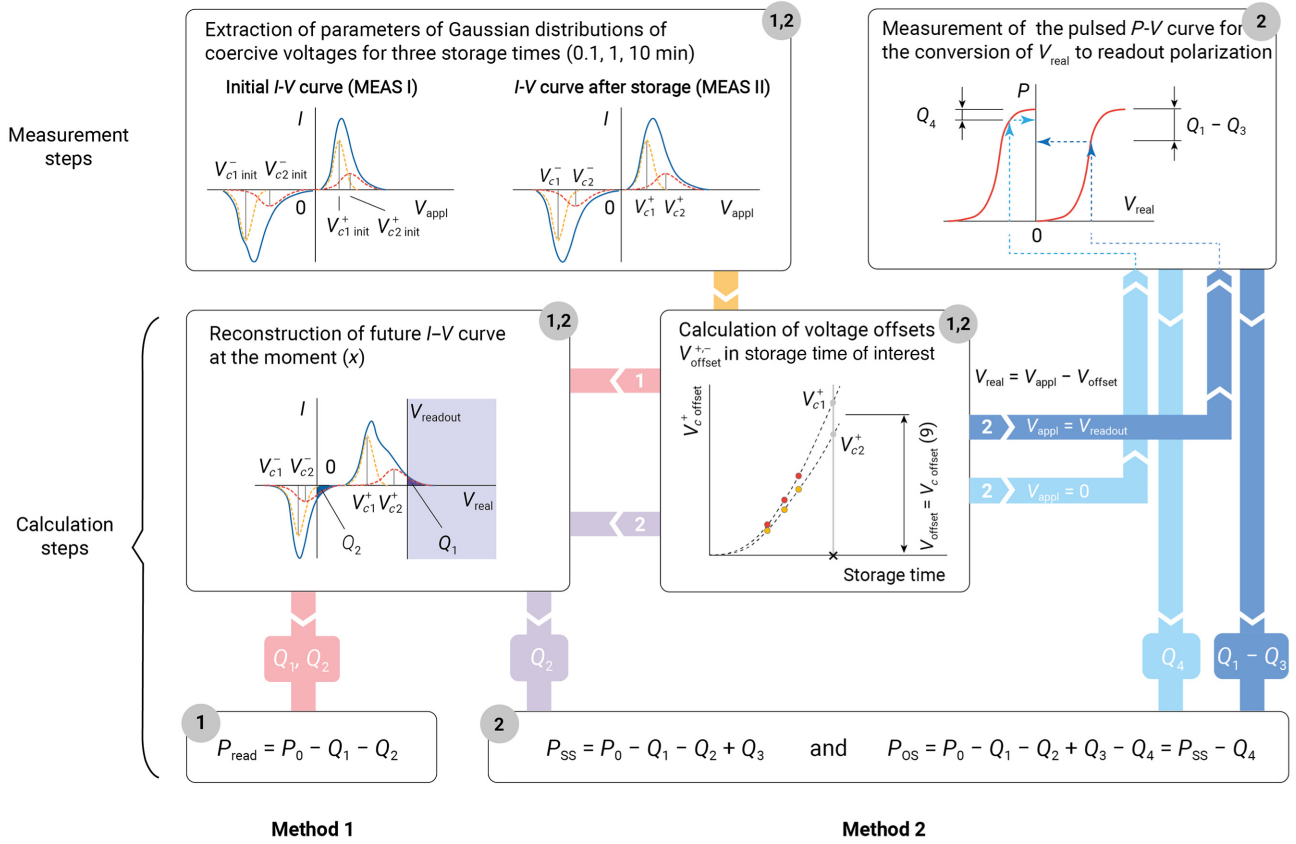


FIG. 6. Algorithms for two methods to calculate the polarization loss, including the express retention test. The numbers 1 and 2 denote the steps required for method 1 (for triangular pulses) and method 2 (for triangular and trapezoidal pulses), respectively.

injection solely, or the interplay of injection and charged-defect migration. As was shown by Tagantsev *et al.* [13], charge injection on its own produces a simple logarithmic dependence of the coercive voltage on time, whereas the two mechanisms cause a dependence that can be empirically described by a quadratic logarithmic dependence. For the final (third) verification of the impact of the interplay of the two mechanisms, we investigate the results of calculation of the polarization readout using the fitting of three experimental voltage offsets by the functions $V_{c\ offset} = V_0 \log(1 + t/t_0)$ and $V_{c\ offset} = V_0 \log^2(1 + t/t_0)$. From Fig. 7(b), it can be seen that fitting by the simple logarithmic function predicts different readout polarizations after a storage time of 10 years, depending on which dataset of storage times is selected. In contrast, when fitted with the quadratic logarithmic function, all three datasets give the same prediction of the retention loss. This result indicates that this function describes well the imprint dynamics over a wide time scale. Indeed, the quadratic logarithmic function works well from 10^{-6} to 10^3 min if we take into account the data in Fig. 3(b). Therefore, on this time scale the imprint dynamics is related to both charge injection and migration of charged-defect traps. It should be noted that with a longer storage time one of

these mechanisms may begin to prevail, and the dynamics of the imprint may change. More studies are required to resolve this issue. Until then, the quadratic logarithmic function provides an upper estimate of the polarization loss corresponding to the worst case.

Because of the high accuracy of the fitting of the imprint dynamics, one can use measurements at short storage times and thus implement an express retention test. Results of the express retention test for OS and SS states are shown in Fig. 7(c). For storage times of 0.1, 1, and 10 min, we acquire current responses using the voltage sequences shown in Fig. 2 and use them to calculate the dependence of the voltage offset on the storage time and thus to calculate the polarization loss over time. The results of calculation for the OS and SS states are presented in Fig. 7(c) as solid lines. In order to compare the results of the calculation with the experimental polarization loss, the readout polarization for storage times of 10, 10^2 , 10^3 , and 10^4 min is experimentally measured, and the experimental points are plotted on the same graph as the calculated curve. For better statistics, for each of these storage times the experimental readout polarization is measured on four separate capacitors, and all acquired experimental points are plotted in Fig. 7(c). One can conclude that the results of the

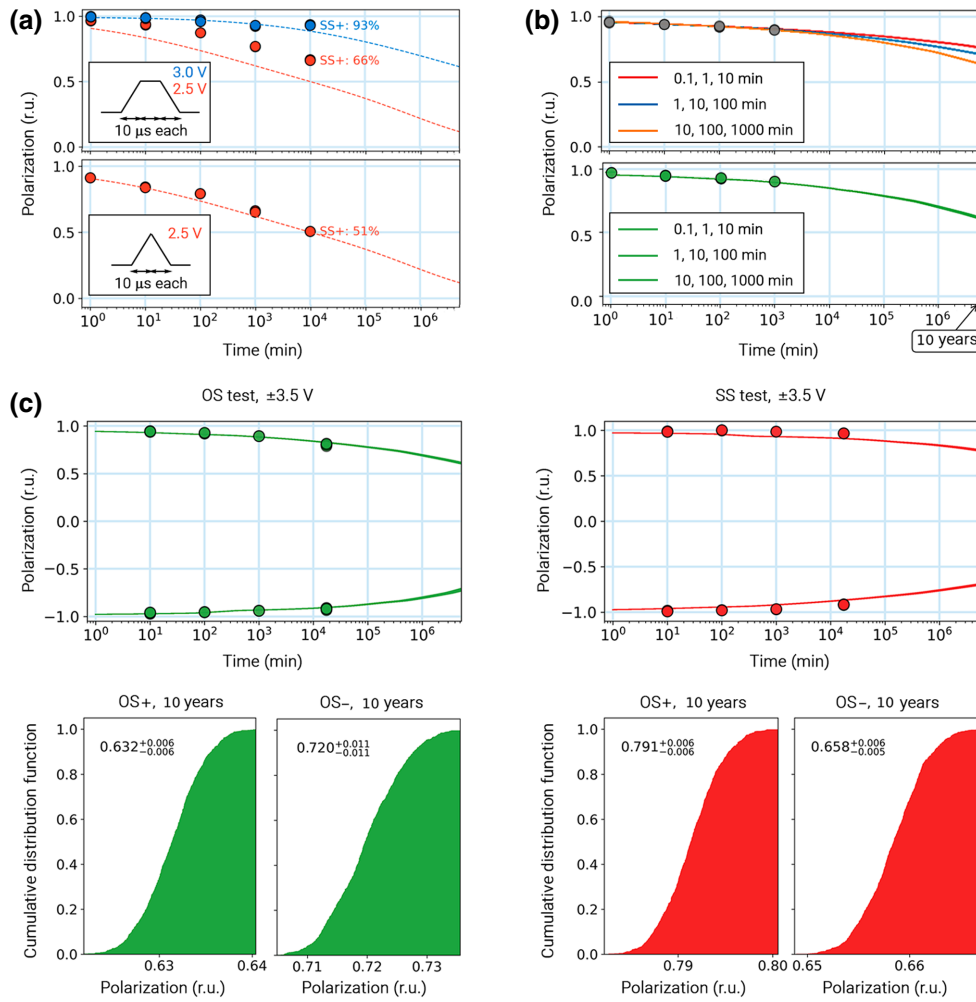


FIG. 7. (a) Result of retention test based on reconstruction of the I - V curve expected after some storage time and further calculation of the read polarization $P_{\text{read}} = P_0 - Q_1 - Q_2$ (first method of calculation of the retention loss). (b) Results of fitting of three different experimental offset points by the functions $V_{c \text{ offset}} = V_0 \log(1 + t/t_0)$ and $V_{c \text{ offset}} = V_0 \log^2(1 + t/t_0)$, and comparison of these results. The insets show the sets of storage times whose current responses MEAS I and MEAS II are used to obtain the I - V curves, calculate the voltage offsets, and thus calculate the polarization loss. (c) Result of the express retention test; storage times 0.1, 1, 10 min. The solid lines are calculated curves; the points are the experimental readout polarization. The experimental points are not used to calculate retention losses; they are given only for comparison of the experimental and calculation results.

calculation are in good agreement with the experimental data on the readout polarization.

To statistically characterize the predicted readout polarization for a 10-year storage time, we use the following method. For each of the three values of t_{delay} (0.1, 1, 10 min) in the voltage sequences in Fig. 2, we measure the current responses MEAS I and MEAS II on four separate capacitors. From the current responses, for each t_{delay} , we obtain four values of the initial coercive voltage $V_{c \text{ init}}$ and four values of the coercive voltage after storage, V_c . For each particular t_{delay} , we take randomly one of the $V_{c \text{ init}}$ and one of the V_c and calculate a coercive-voltage offset $V_{c \text{ offset}}$ for this random pair. In this way, one could obtain 4^4 values of $V_{c \text{ offset}}$ for each t_{delay} , and thus 16^3 combinations for three storage times t_{delay} . We take 10 000 random

combinations of $V_{c \text{ offset}}$, approximate each of them by the quadratic logarithmic function $V_{c \text{ offset}} = V_0 \log^2(1 + t/t_0)$, and calculate the retention loss 10 000 times. In Fig. 7(c) [and in Fig. 7(b) as well], 10 000 calculated numerical dependences of the polarization readout on the storage time are plotted for both OS and SS states. In the same figure, one can see the cumulative distribution functions of the readout polarization in different states after 10 years. To determine the 99.7% confidence interval (which is analogous to 3σ for the normal distribution) for the readout polarization and thus for the retention time of the logical state, we interpolate the discrete cumulative distribution functions to probability levels of 0.997 and 0.003. The numerical results are summarized in Fig. 7(c). For example, one can see that for the OS+ state, half of the

predicted readout polarization values are above $0.632P_0$ and half are below it, and the 99.7% values of the readout polarization fall in the range from $(0.632 - 0.006)P_0$ to $(0.632 + 0.006)P_0$.

IV. CONCLUSIONS

In this paper, we present a retention model that predicts the loss of polarization readout in HfO₂-based FRAM during long-term storage. In this model, we take into account the specific properties of ferroelectric HfO₂. Among them is the different rates of imprint evolution in the two types of film that appear during the crystallization of the HfO₂ film and correspond to two populations of domains in the as-prepared film. The rates are obtained for the two types of film separately, and then an effective coercive voltage is predicted over the storage time. The second feature of ferroelectric HfO₂ underlying the proposed retention test is the interplay of two physical phenomena behind the retention loss, specifically, charge injection into interface traps and migration of charged traps across the functional layer. Because it takes into account the specific properties of ferroelectric HfO₂, the model has high accuracy and thus allows one to predict the retention time for any particular sample in record short time (approximately 1 h, including the time required for computing), whereas usually such prediction takes at least several days. For Hf_{0.5}Zr_{0.5}O₂-based capacitors with small leakage, the retention model shows excellent agreement with experimental results. The approach presented gives a reliable instrument that could help to overcome the main obstacle to commercialization of HfO₂-based memory—the limited retention time.

ACKNOWLEDGMENTS

This work was performed using equipment at the MIPT Shared Facilities Center with financial support from the Russian Science Foundation (Project No. 20-19-00370). The authors are grateful to the ALD group at the MIPT Shared Facilities Center for the growth of the HZO film.

[1] T. S. Böscke, J. Müller, D. Bräuhaus, U. Schröder, and U. Böttger, Ferroelectricity in hafnium oxide thin films, *Appl. Phys. Lett.* **99**, 102903 (2011).

[2] Yu. A. Genenko, J. Glaum, M. J. Hoffmann, and K. Albe, Mechanisms of aging and fatigue in ferroelectrics, *Mater. Sci. Eng.: B* **192**, 52 (2015).

[3] J. A. Rodriguez, K. Remack, K. Boku, K. R. Udayakumar, S. Aggarwal, S. R. Summerfelt, F. G. Celii, S. Martin, L. Hall, and K. Taylor, *et al.*, Reliability properties of low-voltage ferroelectric capacitors and memory arrays, *IEEE Trans. Device Mater. Reliab.* **4**, 436 (2004).

[4] J. Müller, T. S. Böscke, S. Müller, E. Yurchuk, P. Polakowski, J. Paul, D. Martin, T. Schenk, K. Khullar,

and A. Kersch, *et al.*, in *2013 IEEE International Electron Devices Meeting*, p. 10.8.1, 2013.

[5] T. Francois, L. Grenouillet, J. Coignus, P. Blaise, C. Carabasse, N. Vaxelaire, T. Magis, F. Aussenac, V. Loup, and C. Pellissier, *et al.*, in *2019 IEEE International Electron Devices Meeting (IEDM)*, 2019.

[6] J. Okuno, T. Kunihiro, K. Konishi, M. Materano, T. Ali, K. Kuehnel, K. Seidel, T. Mikolajick, U. Schroeder, M. Tsukamoto, and T. Umebayashi, 1T1C FeRAM memory array based on ferroelectric HZO with capacitor under bitline, *IEEE J. Electron Devices Soc.* **10**, 29 (2022).

[7] G. Arlt and H. Neumann, Internal bias in ferroelectric ceramics: Origin and time dependence, *Ferroelectrics* **87**, 109 (1988).

[8] T. Y. Lee, K. Lee, H. H. Lim, M. S. Song, S. M. Yang, H. K. Yoo, D. I. Suh, Z. Zhu, A. Yoon, and M. R. MacDonald, *et al.*, Ferroelectric polarization-switching dynamics and wake-up effect in Si-doped HfO₂, *ACS Appl. Mater. Interfaces* **11**, 3142 (2019).

[9] J. Müller, P. Polakowski, Uwe Schröder, S. Müller, and T. Mikolajick, Ferroelectric hafnium oxide based materials and devices: Assessment of current status and future prospects, *ECS J. Solid State Sci. Technol.* **4**, N30 (2015).

[10] S. Starschich, S. Mentzel, and U. Böttger, Evidence for oxygen vacancies movement during wake-up in ferroelectric hafnium oxide, *Appl. Phys. Lett.* **108**, 032903 (2016).

[11] F. P. G. Fengler, R. Nigon, P. Mural, E. D. Grimley, X. Sang, V. Sessi, R. Hentschel, J. M. LeBeau, T. Mikolajick, and U. Schroeder, Analysis of performance instabilities of hafnia-based ferroelectrics using modulus spectroscopy and thermally stimulated depolarization currents, *Adv. Electron. Mater.* **4**, 1700547 (2018).

[12] M. Grossmann, O. Lohse, D. Bolten, U. Boettger, and R. Waser, The interface screening model as origin of imprint in thin films. II. numerical simulation and verification, *J. Appl. Phys.* **92**, 2688 (2002).

[13] A. K. Tagantsev, I. Stolichnov, N. Setter, and J. S. Cross, Nature of nonlinear imprint in ferroelectric films and long-term prediction of polarization loss in ferroelectric memories, *J. Appl. Phys.* **96**, 6616 (2004).

[14] M. Pešić, S. Slesazek, T. Schenk, U. Schroeder, and T. Mikolajick, Impact of charge trapping on the ferroelectric switching behavior of doped HfO₂, *Phys. Status Solidi (a)* **213**, 270 (2016).

[15] G. D. Wilk, R. M. Wallace, and J. M. Anthony, High-k gate dielectrics: Current status and materials properties considerations, *J. Appl. Phys.* **89**, 5243 (2001).

[16] A. Chouprik, E. Kondratyuk, V. Mikheev, Y. Matveyev, M. Spiridonov, A. Chernikova, M. G. Kozodaev, A. M. Markeev, A. Zenkevich, and D. Negrov, Origin of the retention loss in ferroelectric Hf_{0.5}Zr_{0.5}O₂-based memory devices, *Acta Mater.* **204**, 116515 (2021).

[17] I. Stolichnov, A. K. Tagantsev, E. Colla, N. Setter, and J. S. Cross, Physical model of retention and temperature-dependent polarization reversal in ferroelectric films, *J. Appl. Phys.* **98**, 084106 (2005).

[18] N. Gong, X. Sun, H. Jiang, K. S. Chang-Liao, Q. Xia, and T. P. Ma, Nucleation limited switching (NLS) model for HfO₂-based metal-ferroelectric-metal (MFM)

- capacitors: Switching kinetics and retention characteristics, *Appl. Phys. Lett.* **112**, 262903 (2018).
- [19] A. K. Tagantsev, I. Stolichnov, N. Setter, J. S. Cross, and M. Tsukada, Non-Kolmogorov-Avrami switching kinetics in ferroelectric thin films, *Phys. Rev. B* **66**, 214109 (2002).
- [20] E. Kondratyuk, V. Mikheev, and A. Choupruk, Effect of charge injection on the switching speed of ferroelectric memory based on HfO₂, *ACS Appl. Electron. Mater.* **4**, 3567 (2022).
- [21] J. Rodriguez, K. Remack, J. Gertas, L. Wang, C. Zhou, K. Boku, J. Rodriguez-Latorre, K. R. Udayakumar, S. Summerfelt, T. Moise, D. Kim, J. Groat, J. Eliason, M. Depner, and F. Chu, in *2010 IEEE International Reliability Physics Symposium*, p. 750, 2010.
- [22] S. Müller, J. Müller, U. Schröder, and T. Mikolajick, Reliability characteristics of ferroelectric Si:HfO₂ thin films for memory applications, *IEEE Trans. Device Mater. Reliab.* **13**, 93 (2013).
- [23] A. Choupruk, M. Spiridonov, S. Zarubin, R. Kirtaev, V. Mikheev, Y. Lebedinskii, S. Zakharchenko, and D. Negrov, Wake-up in a Hf_{0.5}Zr_{0.5}O₂ film: A cycle-by-cycle emergence of the remnant polarization via the domain depinning and the vanishing of the anomalous polarization switching, *ACS Appl. Electron. Mater.* **1**, 275 (2019).
- [24] E. D. Grimley, T. Schenk, X. Sang, M. Pešić, U. Schroeder, T. Mikolajick, and J. M. LeBeau, Structural changes underlying field-cycling phenomena in ferroelectric HfO₂ thin films, *Adv. Electron. Mater.* **2**, 1600173 (2016).
- [25] M. Pešić, F. P. G. Fengler, L. Larcher, A. Padovani, T. Schenk, E. D. Grimley, X. Sang, J. M. LeBeau, S. Slezacek, U. Schroeder, and T. Mikolajick, Physical mechanisms behind the field-cycling behavior of HfO₂-based ferroelectric capacitors, *Adv. Funct. Mater.* **26**, 4601 (2016).
- [26] A. Choupruk, D. Negrov, E. Y. Tsymbal, and A. Zenkevich, Defects in ferroelectric HfO₂, *Nanoscale* **13**, 11635 (2021).
- [27] J. Müller, T. Börscke, U. Schröder, S. Müller, D. Braeuhaus, Ulrich Böttger, L. Frey, and T. Mikolajick, Ferroelectricity in simple binary ZrO₂ and HfO₂, *Nano Lett.* **12**, 4318 (2012).
- [28] Y. S. Lin, F. Zeng, S. G. Tang, H. Y. Liu, C. Chen, S. Gao, Y. G. Wang, and F. Pan, Resistive switching mechanisms relating to oxygen vacancies migration in both interfaces in TiN/HfO_x/Pt memory devices, *J. Appl. Phys.* **113**, 064510 (2013).
- [29] S. Zafar, H. Jagannathan, L. F. Edge, and D. Gupta, Measurement of oxygen diffusion in nanometer scale HfO₂ gate dielectric films, *Appl. Phys. Lett.* **98**, 152903 (2011).
- [30] F. P. G. Fengler, M. Pešić, S. Starschich, T. Schneller, C. Künneth, U. Böttger, H. Mulaosmanovic, T. Schenk, M. H. Park, R. Nigon, P. Murali, T. Mikolajick, and U. Schroeder, Domain pinning: Comparison of hafnia and PZT based ferroelectrics, *Adv. Electron. Mater.* **3**, 1600505 (2017).
- [31] S. M. Sze and K. K. Ng, *Physics of Semiconductor Devices*, 3rd Ed. (John Wiley & Sons, New Jersey, 2007).
- [32] V. Mikheev, A. Choupruk, Yu. Lebedinskii, S. Zarubin, A. M. Markeev, A. V. Zenkevich, and D. Negrov, Memristor with a ferroelectric HfO₂ layer: In which case it is a ferroelectric tunnel junction, *Nanotechnology* **31**, 215205 (2020).